Multi-objective optimization for multi-stage constant current charging for Li-ion batteries

Tahir, Muhammad Usman; Sangwongwanich, Ariya; Stroe, Daniel-Ioan; Blaabjerg, Frede

Published in:
Journal of Energy Storage

DOI (link to publication from Publisher):
10.1016/j.est.2024.111313

Publication date:
2024

Document Version
Publisher's PDF, also known as Version of record

Journal of Energy Storage 86 (2024) 111313

Contents lists available at ScienceDirect

Journal of Energy Storage

journal homepage: www.elsevier.com/locate/est

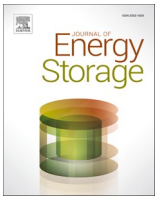

Research Papers

Multi-objective optimization for multi-stage constant current charging for Li-ion batteries

Muhammad Usman Tahir *, Ariya Sangwongwanich, Daniel-Ioan Stroe, Frede Blaabjerg

AAU Energy, Aalborg University, DK-9220 Aalborg, Denmark

ARTICLE INFO

Keywords:
Fast charging
Multi-stage constant current (MSCC)
Electric vehicles (EVs)
Lithium-ion batteries (LIBs)
Multi-objective optimization (MOO)
Constant current constant voltage (CCCV)
Battery performance evaluation

ABSTRACT

Fast charging is a key challenge for the widespread adoption of electric vehicles (EVs), as it can make EVs more convenient and appealing to consumers. Therefore, different charging methods are proposed to enhance the performance of lithium-ion batteries (LIBs). Multi-stage constant current (MSCC) charging can improve LIB's performance in several aspects, including charging time, charged capacity, temperature rise, average temperature rise, and charging energy efficiency. However, achieving a multi-objective performance during LIB charging is challenging. In this paper, the Taguchi method is used to determine the multi-objective optimal (MOO) charging profile for the MSCC charging strategy. The Orthogonal experiments are designed and conducted to find the optimal solutions for each performance parameter for a five-stage constant current (5SCC) charging profile. A comparison is conducted among the performance-based selective charging profiles to validate the optimal charging profile. Furthermore, a comparison is made between the obtained MOO charging profile and the classical equivalent constant current constant voltage (CCCV) method. Experimental results demonstrated that the MOO charging profile reduces the charging time with comparable temperature rise to the CCCV, making it promising for the future alternative efficient EV charging. These findings highlight the effectiveness of the MSCC approach in improving LIB performance.

1. Introduction

The increasing penetration of electric vehicles (EVs) and renewable energy has increased the demand for energy storage technologies. The lithium-ion battery (LIB) is the dominant energy storage solution due to its high power and energy density, minimal self-discharge rate, and long lifespan [1,2]. However, one of the main concerns of LIB operation in EVs is the fast and safe charging. Many fire accidents have been reported during the charging process of EVs in recent years, which are mainly caused by battery overcharging [3,4]. Overcharging the batteries accelerates internal side reactions, including lithium metal plating at the negative electrode [5], composition altering in active material [4], oxidative and reductive decomposition of the electrolyte components [6], and an irreversible degradation of the positive and negative electrode materials due to electrolyte decomposition residues [7]. Therefore, overcharging increases the possibility of thermal runaway. In addition, high-power batteries' substantial magnitude and aggregation amplify the potential for thermal runaway and cascading runaway events [3]. To solve this problem, a new paradigm for an advanced battery management system has emerged: charging optimization for LIBs.

Constant current constant voltage (CCCV) is the traditional strategy for charging commercial LIBs. This strategy comprises two stages: the constant current (CC) stage and the constant voltage (CV) stage. During the CC stage, the charging current (I_{chg}) is kept constant, e.g., at a level that the manufacturer recommends, until the battery voltage reaches a pre-determined limit (V_{max}). In the CV stage, the voltage is maintained at a constant value of V_{max}. At the same time, the charging current is gradually decreased to 5 % of the C-rate. Here, the C-rate refers to the ratio of the charge/discharge current to the nominal rated capacity of the LIB. However, using a high charging current in the CCCV charging method can result in lithium plating, especially when the battery is at a high state of charge (SOC). Lithium plating occurs when the rate at which lithium-ion (Li^{+}) gets embedded in the anode surface is faster than the rate at which it diffuses within the materials [8,9]. This leads to the creation of lithium metal on the anode electrode. This phenomenon can potentially negatively impact the cycle life and the overall performance of LIBs [10]. In literature, several charging strategies have been

* Corresponding author.
E-mail address: mut@energy.aau.dk (M.U. Tahir).

https://doi.org/10.1016/j.est.2024.111313
Received 10 October 2023; Received in revised form 8 February 2024; Accepted 10 March 2024

proposed to tackle these challenges and enhance the lifespan and performance of LIBs. Some examples of different charging methods are pulse charging [11], current-varying charging [12], constant power charging [13], boost charging [14], multi-stage constant current (MSCC) charging [15], and temperature-controlled charging [16]. Among these methods, MSCC charging provides flexibility within the CCCV framework without increasing burdens on battery charger's requirements [17]. The MSCC approach offers several advantages by precisely controlling the charging current in multiple stages. These benefits include enhanced charging efficiency, reduce the risk of lithium plating occurrence [18], and improved battery management overall. To effectively implement the MSCC charging strategy for LIBs [19], three key parameters should be determined: 1) number of stages: the optimal number of stages has been investigated in previous research. It has been observed that the performance of LIBs tends to improve as the number of stages increases from one to five stages, and there may be marginal improvements beyond five stages. 2) Stage transition criteria: various criteria can be used to determine when to do transition between stages during the charging process. The commonly employed transition criteria include: time-based transition, SOC-based transition, cut-off voltage-based transition, and threshold voltage-based transition. The choice of transition criteria depends on the specific requirements and objectives of the charging process. 3) Charging current for each stage: determining the charging current level for each stage can be done through empirical or experimental methods. Typically, high C-rates are selected for the initial stages to expedite charging. Once the predetermined conditions for stage transition are met, the MSCC charging strategy is to switch to a successive stage with lower C-rates. It is important to note that the selection of these factors may vary depending on the specific application, battery chemistry, and desired performance objectives. Researchers often employ empirical or experimental approaches rather than systematic methods to determine the optimal C-rates and transition criteria for each stage of MSCC charging [19,20].

The MSCC charging strategy aims to improve the performance parameters of the LIBs. However, performance parameters, such as charging time and surface temperature rise, may counteract each other when optimizing their performance. In other words, it is not straightforward to optimize all the parameters simultaneously. Therefore, the design of the MSCC charging strategy is, in fact, an optimization problem. Various methods are used in the literature to optimize the MSCC charging current, and previous research has used the Taguchi method and meta-heuristic optimization like particle swarm optimization (PSO) [21], ant colony system [22], genetic algorithm [23], grey golf optimization [24], and numerical optimization [25]. Meta-heuristic optimization tools, known for their stochastic nature and complexity, offer a versatile approach to problem-solving. However, implementing these meta-heuristic approaches requires careful consideration of various problem parameters (i.e., constraints), and their effectiveness may be restricted by high model accuracy [26].

The charging profile of the MSCC strategy can be optimized using a design of experiments (DOE) approach. This approach reduces the reliance on algorithms and models, leading to significant improvements. However, in some previous studies, certain optimization aspects were not fully explored and validated. In [27], the authors utilized the Taguchi method to optimize the charging current for lithium-polymer batteries in four stages with equal SOC-based transitions. However, this study did not perform experiments for unequal SOC intervals and higher levels of C-rate. In [28], the authors employed four four-stage MSCC strategy with the cut-off voltage-based transition. The charging profile is optimized through Taguchi-based PSO to minimize charging time and maximize charged capacity. However, the optimization objective did not consider temperature variation, and different charging profiles were not validated. In [26], the authors optimized the five stages with a cut-off voltage-based transition charging profile. However, the capacity of the complete charged/discharged cycle was not considered. In [29], the authors optimized the charging current for the five stages with cut-off voltage criterion, considering the charging time, charged capacity, and charging energy efficiency as to be optimized. However, temperature variation was not included as an objective parameter. In [30], the authors examined the five stages using unequal SOC-based transition criterion where the experiments were conducted at a maximum of 3C rate. Their analysis did not consider the potential impact of the higher C-rate on the performance parameters and customized optimization. In the above studies, a comparison was made between the optimized results and the CCCV method. However, accurately determining the impact of different C-rates on performance parameters that reflect the physics-based parameters and models for generalizing characteristics of LIBs can be challenging. Overall, while previous studies have made progress in optimizing MSCC charging profiles, there is still a need for further exploration and validation, considering factors such as unequal SOC intervals, temperature variation, and comprehensive evaluation of performance parameters and their customized optimal solutions.

This study investigates the effect of the MSCC charging strategy with unequal SOC levels for lithium-iron-phosphate (LFP) battery cells. The study also investigates the impact of higher C-rates on charging performance. To address this multi-level and multi-factor optimization problem, an optimization algorithm based on the Taguchi technique is employed to find the optimal charging pattern. Using the orthogonal experiment approach significantly reduces the experimental expenditure compared to comprehensive testing methods. The selection of the suitable orthogonal array and updating orthogonal experiments are determined based on the specific parameters. Based on the empirical analysis, the Taguchi method evades the need for complex modeling of LIBs. For analysis, charging efficiency, charging time, charged capacity, surface temperature rise, and average surface temperature rise are considered simultaneous optimal objectives. These objectives are converted into a single optimization problem through weighting factors. Additionally, subjective factors are considered when choosing the optimal solution for a specific optimal profile, not just relying on the objective function. This approach allows for the examination of the influences of the current at each stage on each objective. Moreover, the obtained factor effects can be effectively applied to various charging scenarios, providing flexibility and inspiration for optimal decision-making. Therefore, this approach is well-suited for optimizing the MSCC charging strategy for LIBs, offering valuable insights and practical guidance for achieving improved performance parameters. The effect of the MSCC charging strategy on the battery's lifetime will be evaluated in future publications, considering the optimized charging profiles acquired during the experimental phase.

This paper is structured into five sections. Section 2 introduces the experimental setup and initial performance tests of LIBs. Section 3 looks into the Taguchi method and test procedure in greater detail. It comprehensively describes the methodology and technique employed to collect experimental data for the analysis and optimization procedure. Section 4 presents the results of the experiments and discusses their implications. The findings and insights obtained from the experiments are thoroughly examined and analyzed, shedding light on the relationship between performance parameters and optimal charge patterns. Finally, in Section 5, the paper concludes by summarizing the key findings and contributions of the study. It highlights the significance of the proposed optimal charging pattern and its potential impact on improving the performance of LIBs. Additionally, it suggests potential areas for further investigation in this field.

2. Experimental setup and initial performance tests

2.1. Experimental setup

The experimental setup consists of a host computer (HC), a Neware battery test system (CT-4008-5 V-50 A, ±0.1 % of FS), an auxiliary tester with thermocouple (accuracy: ±0.1 °C), and Memmert temperature

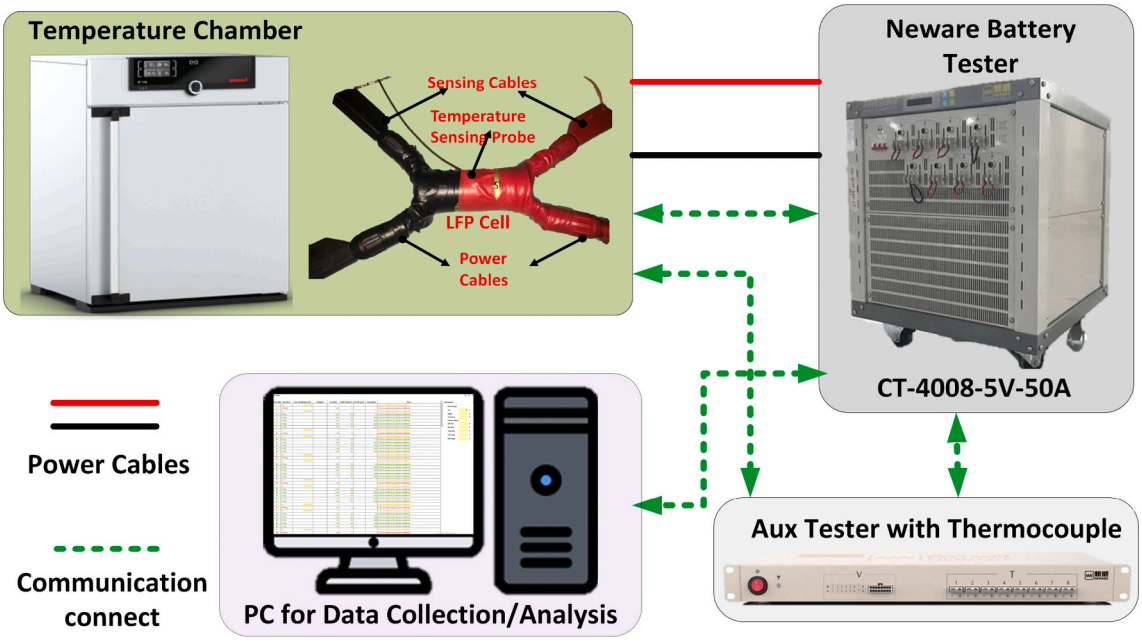

Fig. 1. Experimental setup for implementing multi-stage constant current (MSCC) charging strategy.

Table 1
Lithium-iron-phosphate cell electrical parameters.

Characteristic (units)	Value
Cell type	Cylindrical
Nominal capacity (Ah)	2.6
Nominal voltage (V)	3.3
Cut-off voltage (V)	3.6
Minimum discharge voltage (V)	2
Maximum charge current (A)	10.4
Operating temperature (°C)	−30 to +55
Internal Impedance (1 kHz typical)	6 mΩ

chamber (IF 110, 0.1 °C) as shown in Fig. 1. An $LiFePO_4$ (LFP) battery with a 2.6 Ah rated capacity is used in this work, and Table 1 lists the relevant characteristics of this cell.

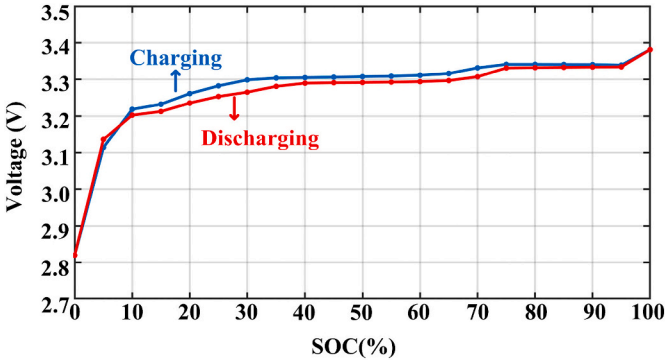

Fig. 2. Dynamic behavior of open circuit voltage (OCV) vs. SOC.

2.2. Initial performance test

The initial performance test includes a preconditioning test and an open circuit voltage (OCV) test. The preconditioning test removes any passivation to which the LIB was subjected between manufacturing and the first test. The OCV test is performed to find the equilibrium voltage levels at different SOC points.

2.2.1. Preconditioning test

The preconditioning test aims to ensure that the battery shows a stable thermo-dynamic behavior. It involves five charge-discharge cycles at a 1C rate and 25 °C. The measured capacity of the LFP battery remained consistent throughout the five cycles, showing a marginal increase of approximately 0.1 %. The test ensures that the battery's capacity remains consistent and does not undergo significant variation exceeding 3 % during two successive discharge cycles [31].

2.2.2. Open circuit voltage (OCV) test

The OCV is the voltage measurement at LIB terminals after a rest period, which depends on operating conditions like SOC, temperature, and materials. LIBs exhibit hysteresis behavior, which may not always correspond to their SOC. This test measures the relationship between OCV and SOC through a constant current (CC) of 0.25C-rate with three

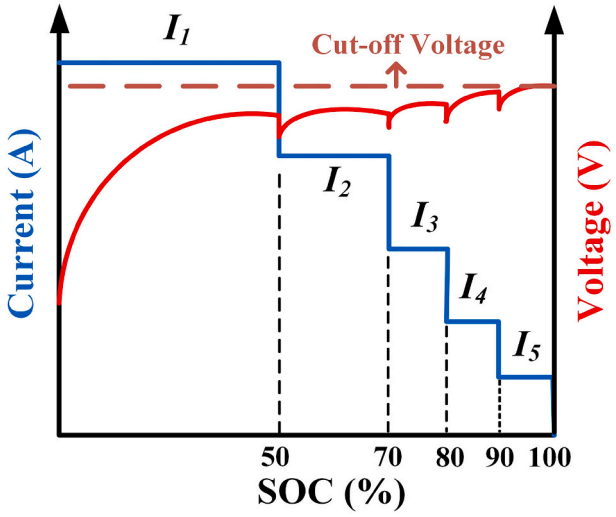

Fig. 3. Typical example of implemented 5SCC charging strategy.

hours of rest time. The OCV-SOC characteristic of the tested LIB, measured at 25 °C with 5 % SOC resolution, is presented in Fig. 2. The hysteresis effect is prominent for 10 %–40 % SOC, and it is intrinsic to LIBs based on LFP active materials.

3. Stage current optimization for MSCC charging strategy

This paper investigates a five-stage constant current (5SCC) charging strategy as the optimization objective. Previous studies show that when the number of charging stages is greater than five, the performance improvements in charging time, energy efficiency, and capacity are marginal [19]. Fig. 3 illustrates the implemented 5SCC charging strategy with SOC-based stage transition.

3.1. Objective function and boundary conditions

A fast-charging strategy can negatively impact the charged/discharged capacity and the maximum/average temperature rise. The energy efficiency during the charging process may also be adversely affected. Therefore, these parameters have been intended as the objective of charging profile optimization. The LIB's quality function consists of five distinct performance parameters: minimizing the charging time (t_{chg}), temperature rise (T_r), and average temperature rise (T_{avg_r}), while maximizing the charging capacity (Q_{chg}) and energy efficiency (η). The quality function is represented in Eq. (1).

$$Quality\ function = w_1 \times t_{chg} + w_2 \times T_r + w_3 \times T_{avg\_r} + w_4 \times Q_{chg} + w_5 \times \eta \quad (1)$$

Here, w_{1-5} are the weighting factors for each performance parameter.

The boundary conditions (i.e., constraint) for the multi-objective current optimization for the mentioned quality function are given below:

$$0.2\ C \le I_5 < I_4 < I_3 < I_2 < I_1 \le 4\ C \quad (2)$$

$$0.4\ h \le t_{chg} \le 0.9\ h \quad (3)$$

$$25^{\circ}C \le T_r \le 45^{\circ}C \quad (4)$$

$$25^{\circ}C \le T_{avg_r} \le 40^{\circ}C \quad (5)$$

$$0\ Ah < Q_{chg} \le 2.6\ Ah \quad (6)$$

$$90\% \le \eta \le 100\% \quad (7)$$

$$2\ V \le V_T \le 3.6\ V \quad (8)$$

The upper charging current rate is set at 4C, and the lower charging current limit is 0.2C in this current optimization problem, as also shown in Eq. (2). The charging current decreases monotonically from stage one to five. The current charging rate is selected based on the performance parameters as shown in Eqs. (3)–(7). The charging time constraint is set from 0.4 h to 0.9 h. The upper limit of the average and surface temperature rise is set to 40 °C and 45 °C, respectively. These temperature boundaries ensure that LIB charging and discharging tests are performed within a controlled thermal environment. The boundary condition for the charging capacity (Q_{chg}) is defined as Eq. (6), which means that the charging quantity must be >0 Ah, indicating that the battery is being charged and should not exceed 2.6 Ah. The upper limit of 2.6 Ah is set to prevent overcharging the battery beyond a safe and optimal level. Exceeding this limit could lead to expedited degradation, reduced cycle life, and safety risks.

The boundary condition for the charging efficiency (η) is shown in Eq. (7). The lower limit of 90 % is set to ensure that the charging and discharging processes are reasonably efficient. LIB terminal voltage (V_T) limits are set during the charging and discharging process to prevent under-discharging and overcharging, as shown in Eq. (8). The lower limit of 2 V is set to ensure that the battery maintains a minimum voltage level for proper operation. Falling below this limit may indicate an over-discharged battery, negatively affecting its performance and lifetime while at the same time affecting its safe operation. The upper limit of 3.6 V is established to prevent overvoltage conditions that can potentially damage the battery. Exceeding this limit may lead to accelerated aging, electrolyte decomposition, or even safety hazards.

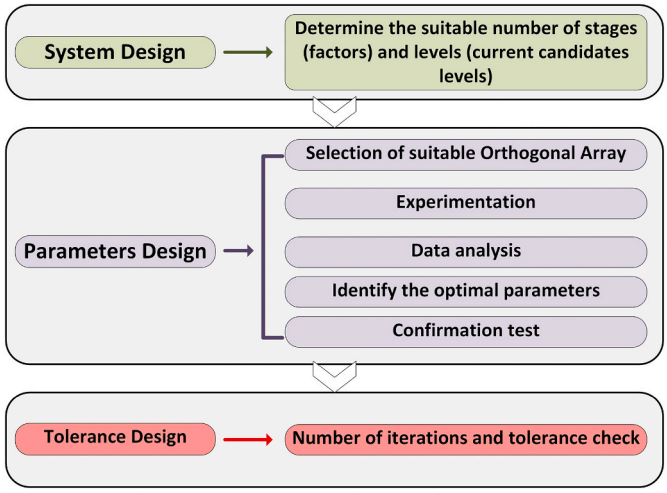

Fig. 4. Optimization steps using Taguchi technique.

3.2. Experimental design using Taguchi optimization

The Taguchi method employs a DOE approach to analytically investigate the influence of various charging parameters at the performance of LIBs. The Taguchi technique aims to identify optimal patterns for a specific set of control variables by conducting a limited number of experiments. The experimental design intends to achieve a balanced outcome by ensuring that different levels of distinct factors are given equal opportunities. This approach ensures that each factor is weighted equally in the overall design of the experiment. It enables the evaluation of how a system's output responds to varying levels of control factors. Optimizing the design for robustness is to minimize the impact of the performance parameter variations. This method analyzes performance data, and the optimal parameters are determined using orthogonal arrays (OAs), signal-to-noise (S/N) ratios, and their mean effect of the charging current level on performance parameters [32].

The Taguchi method is used to optimize the charging current of the MSCC for LIBs. Utilizing this technique, a limited number of experiments is needed to evaluate all possible parameter combinations, saving resources and time. The method described in this study allows for the simultaneous optimization of multiple charging parameters, considering their interactions and how they affect the battery performance. The Taguchi method aims to achieve robustness in the charging profile design process, ensuring consistent and reliable battery performance. This minimizes the potential for under-charging, over-charging, and over-heating.

The key idea is to develop a design with minimal sensitivity that can optimize the output variables regardless of random variation in input variables within predetermined thresholds. This process includes the following steps: 1) system design, 2) parameter design, and 3) tolerance design, as shown in Fig. 4 [33]. The system design process includes the selection of input and output variables. In this scenario, the C-rate for each stage is considered as an input variable, while the LIB performance parameters (e.g., charging time, energy efficiency, etc.) are outputs. The current levels for each candidate stage are designed during the parameter design phase. The tolerance design is the last step of the process. The present study focuses on LIB's tolerance design and explicitly examines

Table 2
Factor level table for optimizing the respective current candidate level at each stage.

Level	Factors (C-rate)				
	S_1	S_2	S_3	S_4	S_5
L_1	$I_{1,1}$	$I_{2,1}$	$I_{3,1}$	$I_{4,1}$	$I_{5,1}$
L_2	$I_{1,2}$	$I_{2,2}$	$I_{3,2}$	$I_{4,2}$	$I_{5,2}$
L_3	$I_{1,3}$	$I_{2,3}$	$I_{3,3}$	$I_{4,3}$	$I_{5,3}$
L_4	$I_{1,4}$	$I_{2,4}$	$I_{3,4}$	$I_{4,4}$	$I_{5,4}$

Table 3
Implemented orthogonal array for experimental analysis.

Experiments	S_1	S_2	S_3	S_4	S_5
1	$I_{1,1}$	$I_{2,1}$	$I_{3,1}$	$I_{4,1}$	$I_{5,1}$
2	$I_{1,1}$	$I_{2,2}$	$I_{3,2}$	$I_{4,2}$	$I_{5,2}$
3	$I_{1,1}$	$I_{3,2}$	$I_{3,3}$	$I_{4,3}$	$I_{5,3}$
4	$I_{1,1}$	$I_{4,2}$	$I_{3,4}$	$I_{4,4}$	$I_{5,4}$
5	$I_{1,2}$	$I_{2,1}$	$I_{3,2}$	$I_{4,3}$	$I_{5,4}$
6	$I_{1,2}$	$I_{2,2}$	$I_{3,1}$	$I_{4,4}$	$I_{5,3}$
7	$I_{1,2}$	$I_{3,2}$	$I_{3,4}$	$I_{4,1}$	$I_{5,2}$
8	$I_{1,2}$	$I_{4,2}$	$I_{3,3}$	$I_{4,2}$	$I_{5,1}$
9	$I_{1,3}$	$I_{2,1}$	$I_{3,3}$	$I_{4,4}$	$I_{5,2}$
10	$I_{1,3}$	$I_{2,2}$	$I_{3,4}$	$I_{4,3}$	$I_{5,1}$
11	$I_{1,3}$	$I_{3,2}$	$I_{3,1}$	$I_{4,2}$	$I_{5,4}$
12	$I_{1,3}$	$I_{4,2}$	$I_{3,2}$	$I_{4,1}$	$I_{5,3}$
13	$I_{1,4}$	$I_{2,1}$	$I_{3,4}$	$I_{4,2}$	$I_{5,3}$
14	$I_{1,4}$	$I_{2,2}$	$I_{3,3}$	$I_{4,1}$	$I_{5,4}$
15	$I_{1,4}$	$I_{3,2}$	$I_{3,2}$	$I_{4,4}$	$I_{5,1}$
16	$I_{1,4}$	$I_{4,2}$	$I_{3,1}$	$I_{4,3}$	$I_{5,2}$

the 0.05C rate. The objective is to minimize the cost of experimentation while simultaneously determining the most efficient multi-objective optimal (MOO) solution.

3.2.1. Selection of suitable orthogonal array

The selection of the charging current for each stage is determined by the design of the OAs. The OA design consists of factors and levels. The five factors considered correspond to the five charging stages, each with four distinct levels. This means that the charging current for each stage will be optimized based on these four distinct levels. The highest charging C-rate permitted by the manufacturer is 4C, which is then divided by 20 to distribute the levels evenly, resulting in each level having a 0.2C interval. Thus, L_{16} is selected as the optimal OA for a balanced partial factorial design with 16 experiments. The general representation of the OA is $OA_n(s^m)$, where n denotes to the number of experiments, and s and m corresponds to the number of levels and factors, respectively. Table 2 illustrates the factor level table, and Table 3 shows the implemented OA table.

The chosen OA design aims to minimize the number of experiments required while still capturing the effects of the various parameters on the performance characteristic. It follows a balanced partial factorial design approach, shown in previous research [33], to yield comparable results to those obtained from full factorial designs. Using the OA, the effects of different parameters on performance characteristics can be evaluated in a more efficient and reduced order of experiments.

3.2.2. Test procedure

The LIB cell is charged using the 5SCC charging strategy at 25 °C. A higher C-rate charging at the lower level of SOC has less effect on the degradation of the LIB's electrode material, SEI, and lithium-plating. Therefore, the LIB is charged between 0 %–50 % SOC in the first stage. During the second stage, the battery is charged between a 50 %–70 % SOC level. The remaining 30 % SOC is charged with a 10 % SOC interval in the last three stages. All experiments are conducted in accordance with the defined SOC levels, as shown in Fig. 3. The test procedure for the implemented 5SCC charging strategy is shown in Fig. 5.

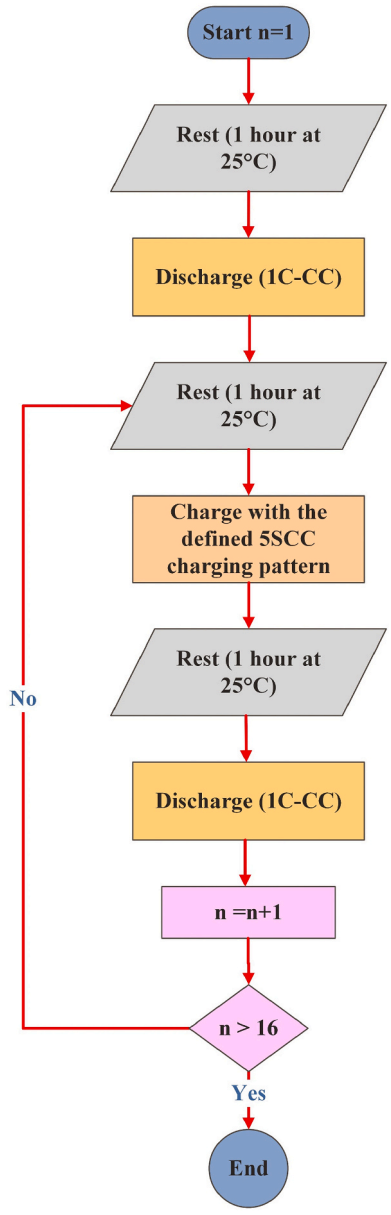

Fig. 5. Experimental procedure for the implemented 5SCC charging strategy using L_{16} orthogonal array.

3.3. Data analysis

By analyzing the experimental data, the optimization of each stage can be determined through sixteen experiments. Two variations are considered: the fluctuation of each factor's level and the weight of each effect. The expression for the variation of the five objectives with factor level is denoted as $\overline{x_{I_{f,l}}}$, as described in Eq. (9).

$$\begin{cases} \overline{x_{I_{f,l}}} = \dfrac{1}{4}\displaystyle\sum_{n=1}^{16}\{x_{I_{f,l}}(n)\} \\ f = 1,2,3,4,5 \\ l = 1,2,3,4 \end{cases} \tag{9}$$

The variable x represents the quality function parameters or performance parameters obtained from the experiments. The variable I describes the current value based on the associated factor F and factor

Table 4
Factor level table for first orthogonal experiments.

Level	Factors (values are in C-rate)				
	S_1	S_2	S_3	S_4	S_5
L_1	4	3.2	2.4	1.6	0.8
L_2	3.8	3	2.2	1.4	0.6
L_3	3.6	2.8	2	1.2	0.4
L_4	3.4	2.6	1.8	1.0	0.2

level l. The true value of $I_{f,l}$ is characterized by the average value denoted as ($\overline{x_{I_{f,l}}}$). This average value represents the average performance parameter associated with a specific factor and factor level.

The S/N ratio is employed to analyze the impact of the five current stages, each having four candidate levels. Within the context of the Taguchi method, this ratio is utilized to assess the influence of individual factors and their respective levels on the quality function. In this study, the performance parameters are considered as quality parameters, and the optimization function is defined as the quality function. The derivation of the S/N ratio is as follows:

$$S\Big/N_{qp_{fl}} = \begin{cases} -10log\left(\frac{1}{n}\sum_{j=1}^{n}\left(y_{fl}^{2}\right)\right), & STB \\ -10log\left(\frac{1}{n}\sum_{j=1}^{n}\left(y_{fl}^{-2}\right)\right), & LTB \end{cases} \tag{10}$$

In the context of the S/N ratio calculation, several variables are involved. n represents the total number of samples, j denotes the specific sample, and y_{fl} corresponds to the experimental observations associated with factors and levels. qp represents the quality parameter (e.g., t_{chg}) The Taguchi method employs the concept of mean squared deviation to determine the S/N ratio. The calculation of the S/N ratio depends on whether the response falls under the category of "smaller the better" (STB) or "larger the better" (LTB). STB indicates a response where lower values are desirable, while LTB signifies a response where higher values are preferred. In this study, the charging time and max/avg. temperature rise are classified as STB-type response parameters, while energy efficiency and charged capacity are categorized as LTB-type responses within the quality function.

Once the S/N ratio has been calculated, the mean of each quality parameter is determined using Eq. (9). This mean value is referred to as the average S/N ratio. Considering the mean effect of the S/N ratio, the impact of each factor is assessed using a weighting strategy to optimize the current level accordingly. The normalized values of each quality parameter for each factor and its level are obtained using Eq. (11) to assist this process. Normalization allows for a standardized comparison and evaluation of the effects of different factors on the overall quality parameters.

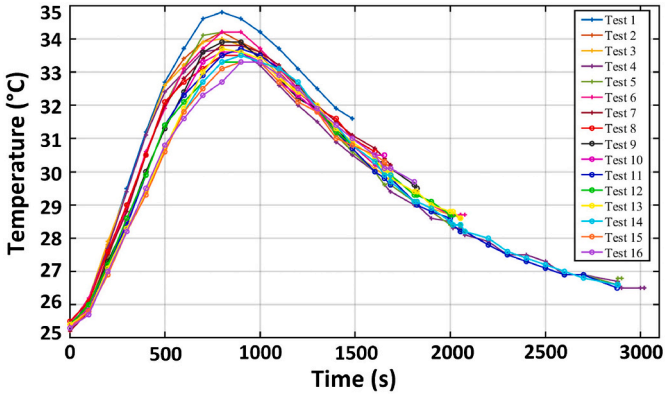

Fig. 6. Temperature variation for the first Orthogonal array experimentation.

$$W_{\overline{S/N_{I_{f,l}}}} = \begin{cases} \frac{\overline{S/N_{I_{f,l}}}}{max\left(\overline{S/N_{I_{f,l}}}\right)}, & LTB \\ \frac{max\left(\overline{S/N_{I_{f,l}}}\right)}{\overline{S/N_{I_{f,l}}}}, & STB \end{cases} \tag{11}$$

Various approaches can be employed to find the optimal charging pattern. The charging pattern can be customized using the Taguchi method based on the specific parameter we aim to optimize. A weight strategy is also applied to determine the MOO pattern, with equal weights or unequal weights assigned to different quality parameters. This paper uses the equal weight strategy to identify the MOO charging profile, ensuring that each performance parameter is given equal importance in the optimization process.

4. Result and discussion

4.1. First orthogonal experiment

The Taguchi orthogonal experiments are conducted according to the procedure outlined earlier. The factor level table for the first orthogonal experiments is illustrated in Table 4. The experimental observations are presented in Table 5. The charging time, charged capacity, surface temperature, and average temperature rise are directly measured using the battery testing station. However, the charging energy efficiency is

Table 5
Experimental observations and their S/N ratio.

Exp. no.	Observations (units)					S/N ratio (dB)				
	Time (s)	Capacity (Ah)	Efficiency (%)	Temp. rise (°C)	Avg. temp. rise (°C)	Time	Capacity	Efficiency	Max_Temp	Avg_Temp
1	1475	2.585	92.42	34.8	31.9	−63.376	8.250	39.315	−30.832	−30.076
2	1677	2.585	93.05	34.3	31.4	−64.491	8.249	39.375	−30.706	−29.936
3	2043	2.586	93.29	34.1	30.9	−66.205	8.252	39.397	−30.655	−29.802
4	3008	2.583	93.64	33.7	29.6	−69.566	8.242	39.429	−30.553	−29.420
5	2891	2.585	93.56	34.2	29.8	−69.221	8.249	39.422	−30.681	−29.484
6	2067	2.581	93.51	34.4	30.6	−66.307	8.236	39.417	−30.731	−29.709
7	1677	2.580	93.33	33.9	31.3	−64.491	8.232	39.400	−30.604	−29.908
8	1594	2.574	93.36	33.7	31.2	−64.050	8.212	39.403	−30.553	−29.875
9	1755	2.577	93.40	33.9	30.9	−64.886	8.222	39.407	−30.604	−29.805
10	1645	2.573	93.42	33.6	31.0	−64.323	8.209	39.409	−30.527	−29.816
11	2867	2.581	93.77	33.8	29.6	−69.149	8.236	39.441	−30.578	−29.432
12	2004	2.581	93.63	33.5	30.6	−66.038	8.236	39.428	−30.501	−29.717
13	2046	2.579	93.73	33.7	30.5	−66.218	8.229	39.438	−30.553	−29.697
14	2872	2.580	93.87	33.5	29.6	−69.164	8.232	39.451	−30.501	−29.411
15	1711	2.571	93.58	33.5	30.7	−64.665	8.202	39.424	−30.501	−29.734
16	1802	2.575	93.63	33.5	30.7	−65.115	8.216	39.428	−30.501	−29.729

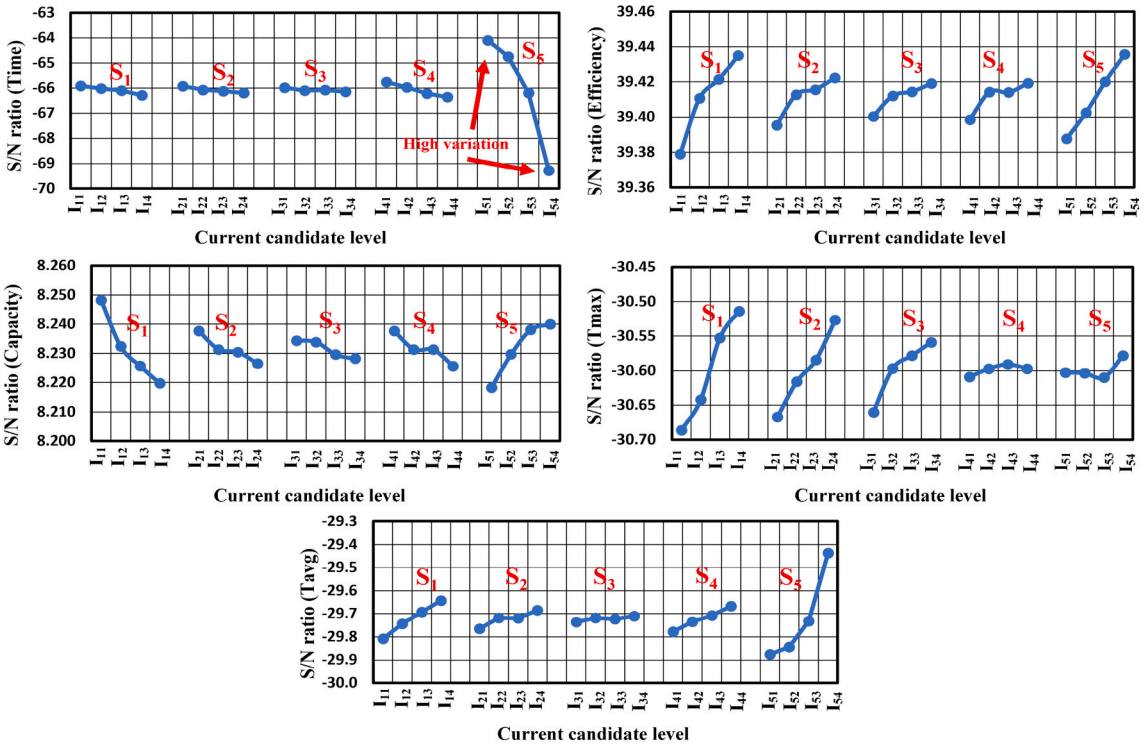

Fig. 7. Average S/N values of each current candidate for each performance parameters in the first OA experiments.

calculated by determining the ratio of the energy extracted during discharge to the charged capacity from the charging process, as shown in Eq. (12). This calculation allows for evaluating the energy efficiency of the charging process.

$$\eta\,(\%) = \frac{I_d \times t_d}{\sum_{j=1}^{n} I_{c,j} \times t_{c,j}} \tag{12}$$

In Eq. (12), the variables I_d, t_d, n, I_c, and t_c represent the discharging current, discharging time, number of stages, charging current, and charging time, respectively. The S/N ratios for these variables are calculated using Eq. (10), as illustrated in Table 5.

According to Table 5, experiment number 1 has the shortest charging time but the lowest energy efficiency, higher surface temperature, and average temperature rise. Conversely, experiment number 4 has the longest charging time but the lowest average temperature rise during charging. Fig. 6 shows the temperature variations observed in the conducted experiments. The surface temperature rise differs, and the speed of temperature rise depends on the currents applied in the first and second stages. Higher currents in these stages result in a greater surface temperature rise. It can be visible in all tested experiments. The subsequent stages have lower current values, leading to a decrease in the surface temperature. For example, the temperature rise in test 1 reached 34.8 °C in the second stage; it decreased due to a lower C-rate in the following stages. Therefore, optimizing the charging current for each stage is crucial to enhance the overall performance of LIBs. The average S/N ratio for each current level associated with each current factor is calculated using Eq. (9). The mean values of each current level and stage for each performance parameter is presented in Fig. 7, where the mean values of charging time, charged capacity, charging energy efficiency, surface temperature rise, and average temperature rise are shown. It can also be seen from Fig. 7 that the fifth stage exhibits the highest variation in charging time. This indicates that in Stage 5, level 1 current takes less time to charge than level 4 current. Similarly, the mean effects of each performance parameter at each current level and stage can be observed. Due to the variation in each current level and stage, optimization based on user preferences or application requirements becomes crucial. Hence, a weighting strategy is implemented to obtain a MOO charging pattern that considers all performance parameters trade-offs equally. The average S/N ratio is normalized using Eq. (11) to assign weights to each performance parameter. The normalized average values for each performance parameter are presented in Table 6.

The quality function for this optimization problem is defined in Eq. (1), and a weight of 0.2 is assigned to each performance parameter. The level weights are presented in Table 6. The values highlighted in red color represent the MOO pattern for the first orthogonal experiments. The optimal pattern for the first orthogonal experiments is 3.6C, 2.6C, 2C, 1.6C, and 0.8C from Stage 1 to Stage 5, respectively.

4.1.1. *Customized optimization for each performance parameter*

The first orthogonal set of experiments permits the customization of the charging profile in accordance with particular performance parameters. Table 6 illustrates the normalized average S/N ratio for each performance parameter. The charging profile can be derived from the average S/N ratio for charging time if, for example, an EV user prioritizes faster charging without much regard for other parameters. In Stages 1 through 5, the first level of current reduces the charging time. Therefore, the charging profile that reduces charging time should be chosen. Regarding charging time, the optimal charging profile for Stages 1 through 5 in this scenario would be 4C, 3.2C, 2.4C, 1.6C, and 0.8C, respectively. Similarly, it is possible to obtain optimal patterns for other performance parameters as well. The optimal charging profile for each performance parameter is presented in Table 7. In addition, these optimized performance profiles undergo experimental validation.

To evaluate the charging profile of the selectively optimized performance parameters, validation experiments were conducted at a temperature of 27 °C. To maintain consistency with earlier experiments, the current experiments utilized the same LFP battery, along with the same testing procedures and experimental conditions. Fig. 8 depicts the variations in voltage, optimized current patterns, and temperature for every performance parameter and MOO. The temperature rise behavior is consistent across all experiments, with the capacity charging profile

Table 6
Identifying the optimal charge profile (red color) for considering equal weights of all performance parameters.

Response (dB)	Levels	Factors				
		S1	S2	S3	S4	S5
Chg.Time	L1	1.0000	1.0000	1.0000	1.0000	1.0000
	L2	0.9984	0.9978	0.9982	0.9968	0.9901
	L3	0.9971	0.9969	0.9986	0.9932	0.9684
	L4	0.9943	0.9960	0.9975	0.9911	0.9254
Chg.Cap	L1	1.0000	1.0000	1.0000	1.0000	0.9974
	L2	0.9981	0.9992	0.9999	0.9992	0.9988
	L3	0.9973	0.9991	0.9994	0.9992	0.9998
	L4	0.9966	0.9986	0.9993	0.9985	1.0000
Chg.eff	L1	0.9986	0.9993	0.9995	0.9995	0.9988
	L2	0.9994	0.9998	0.9998	0.9999	0.9992
	L3	0.9997	0.9998	0.9999	0.9999	0.9996
	L4	1.0000	1.0000	1.0000	1.0000	1.0000
T.max	L1	0.9944	0.9954	0.9967	0.9994	0.9992
	L2	0.9958	0.9971	0.9988	0.9998	0.9992
	L3	0.9987	0.9981	0.9994	1.0000	0.9990
	L4	1.0000	1.0000	1.0000	0.9998	1.0000
T.avg	L1	0.9944	0.9973	0.9991	0.9963	0.9853
	L2	0.9966	0.9989	0.9997	0.9977	0.9863
	L3	0.9983	0.9989	0.9996	0.9986	0.9901
	L4	1.0000	1.0000	1.0000	1.0000	1.0000
Level weights	L1	0.9975	0.9984	0.9991	0.9990	0.9961
	L2	0.9976	0.9986	0.9993	0.9987	0.9947
	L3	0.9982	0.9986	0.9994	0.9982	0.9914
	L4	0.9982	0.9989	0.9994	0.9979	0.9851

exhibiting the highest temperature increase. Table 7 shows the normalized experimental results based on selective charging profiles. In addition, it demonstrates the wide variation in charging time. Due to higher C-rates in all stages, the time charging profile has the shortest charging time compared to other charging patterns. Furthermore, this charging profile exhibits a significant increase in temperature.

Moreover, the charged capacity of LIB remains approximately the same in every case. The maximum difference in charged capacity is 1.2 %. Further, the charging profile for energy efficiency has the highest energy efficiency and the lowest average temperature rise compared to other charging profiles because the first and last charging C-rates are the lowest. Based on the extensive analysis conducted, it can be concluded that the Taguchi method effectively optimizes the charging profile by employing a condensed set of experiments that are specifically designed to meet individual customization needs.

4.2. Second orthogonal experiment

The performance variation in the first set of experiments is relatively wide due to the large C-rate step in each stage level. Therefore, the second set of orthogonal experiments is designed based on the experimental results and findings from the first OA. Thus, Table 4 is updated. The second orthogonal experiment aimed to reduce the C-rate between the current candidate levels to further optimize the performance parameters. In Stage 1, it was determined that the optimal level was 3.6C. In the second orthogonal experiment, the difference between two consecutive levels was reduced to 0.1C and 0.05C, narrowing down the interval from 0.2C. To ensure accuracy, the tolerance design in this study was set at 0.05C. Following a similar approach to Stage 1, the second orthogonal experiments were designed, and the corresponding experimental settings are provided in Table 8. Table 3 remains unchanged, and the experiments were conducted following the previously defined procedure. The results of these experiments are presented in Table 9. It can be observed that the variation in performance parameters in this set of experiments has been reduced compared to the first orthogonal experiments.

Table 9 shows that experiment no. 1 achieved the shortest charging time of 1516 s but with the lowest energy efficiency of 92.80 %. Experiment no. 2 recorded the highest surface temperature of 36.4 °C and the highest average surface temperature of 33.9 °C. Experiment no. 14 demonstrated the highest energy efficiency of 93.42 %. The difference between the minimum and maximum charging time is approximately 164 s. Similarly, there is a difference of about 2.2 °C in surface temperature and around 0.62 % in energy efficiency. Notably, the charging capacity remains nearly constant across all experiments.

Fig. 9 illustrates the average S/N ratio of each current candidate for each performance parameter after the computation of the S/N ratio from the experimental observation. Fig. 9 shows that Stage 5 has the highest variation in charging time compared to other stages. A similar effect of different current candidates' levels at each stage can be seen. From Fig. 9, the optimal pattern for each performance parameter can be obtained. The customized optimal charging profile is possible using the average S/N plots. The details of the customized optimal charging pattern are discussed later.

After normalizing the data using a methodology similar to the first orthogonal experiment, it is possible to get an optimal charging profile that optimizes all performance parameters equally. Thus, the optimal charging profile from the second orthogonal set of experiments is 3.5C, 2.5C, 1.9C, 1.7C, and 0.9C for Stage 1 to Stage 5, respectively.

4.2.1. Customized optimization of performance parameters

The second set of orthogonal experiments is conducted to fine-tune the charging profile based on specific performance parameters. The average S/N values corresponding to individual performance parameters are depicted in Fig. 9. Like the abovementioned procedure, optimal patterns for each performance parameter can be derived. Table 10 illustrates the desired charging profile for each performance parameter. Furthermore, these refined performance profiles underwent empirical validation, which was carried out at a temperature of 27 °C to evaluate the charging profile with selectively enhanced performance parameters. The presented study used the same LFP battery, testing protocols, and experimental conditions to ensure methodological consistency with prior investigations, as mentioned above. Fig. 10 represents voltage variations, optimal current patterns, and temperature variations across all performance metrics and MOO charging profiles. The observed temperature increase remains consistent across all conducted experiments, with the capacity-focused charging profile exhibiting the highest temperature rise. Normalized experimental results based on the chosen charging profiles are shown in Table 10, which highlights the substantial difference in the required charging times. The time-based charging profile leads to minimized charging time due to higher C-rates in all stages compared to the other charging patterns.

Furthermore, the time-based charging profile shows a significant temperature rise. The LIB's charged capacity remains constant across all scenarios, with a maximum deviation of 0.2 %. Notably, regarding

Table 7
Comparison among selective performance based optimized charging profiles.

Charge method	Charge current (C-rate)		Charge time (%)	Charged capacity (%)	Energy efficiency (%)	Avg. temp. rise (%)	Max. temp. rise (%)
Time	S1	4	100.0 %	98.8 %	99.0 %	165.3 %	120.0 %
	S2	3.2					
	S3	2.4					
	S4	1.6					
	S5	0.8					
Charged capacity	S1	4	193.3 %	100.0 %	99.2 %	118.5 %	121.7 %
	S2	3.2					
	S3	2.4					
	S4	1.6					
	S5	0.2					
Energy efficiency, and avg. temp	S1	3.4	214.6 %	99.4 %	100.0 %	100.0 %	103.3 %
	S2	2.6					
	S3	1.8					
	S4	1					
	S5	0.2					
Max. temp	S1	3.4	211.5 %	99.5 %	99.3 %	102.6 %	100.0 %
	S2	2.6					
	S3	1.8					
	S4	1.2					
	S5	0.2					
MOO profile	S1	3.6	110.5 %	99.4 %	99.5 %	139.3 %	103.3 %
	S2	2.6					
	S3	2					
	S4	1.6					
	S5	0.8					

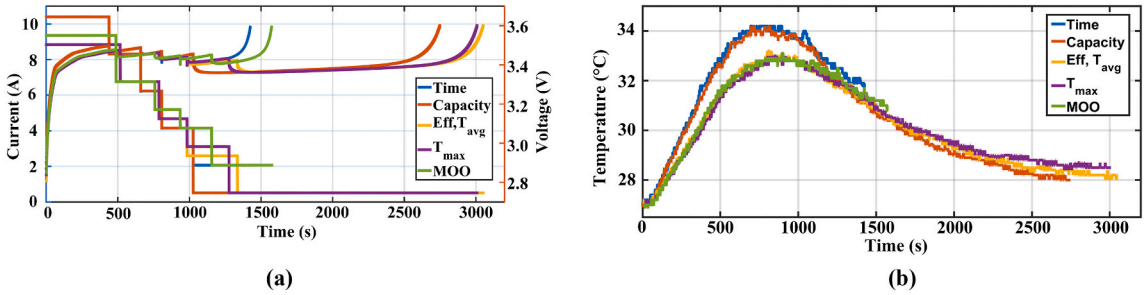

Fig. 8. Comparison of performance-based selective parameter charging profiles (charging time, capacity, Efficiency, T_{avg}, T_{max} and MOO charging) from first orthogonal set of experiments a) waveforms of battery voltage and implemented current levels for each performance parameter, b) demonstrating the optimization process's effect on battery temperature dynamics.

Table 8
Factor level table for second orthogonal experiments.

Level	Factors (values are in C-rate)				
	S_1	S_2	S_3	S_4	S_5
L_1	3.7	2.7	2.1	1.7	0.9
L_2	3.65	2.65	2.05	1.65	0.85
L_3	3.6	2.6	2	1.6	0.8
L_4	3.5	2.5	1.9	1.5	0.7

energy efficiency, the charging profile demonstrates superior efficiency and the least average temperature increase compared to other charging profiles. This is attributed to utilizing the lowest initial and final charging C-rates. Based on the comprehensive research conducted, it can be deduced that the Taguchi technique effectively optimizes the charging profile through a concise set of experiments tailored to address specific customization needs.

4.3. Comparison with CCCV

To validate the charging profile obtained from MOO, validation experiments were conducted comparing the MOO charging profile with an equivalent CCCV charging profile at temperatures of 25 °C and 35 °C. In the equivalent CCCV charging, the current in the CC mode was set at 5.9 A, with a cut-off current of 0.13 A in the CV mode. The experimental procedure remained consistent with the previously discussed approach.

The experimental results are summarized in Table 11. The results

Table 9
Second orthogonal experiments observations.

Ex no.	Time (s)	Capacity (Ah)	Efficiency (%)	Temp. rise (°C)	Avg. temp. rise (°C)
1	1516	2.587	92.80	36.0	33.4
2	1547	2.583	93.35	36.4	33.9
3	1586	2.581	93.34	35.8	33.4
4	1681	2.581	93.39	35.1	32.8
5	1637	2.58	93.37	35.1	32.6
6	1587	2.577	93.34	34.9	32.4
7	1558	2.577	93.27	34.8	32.3
8	1542	2.576	93.31	34.8	32.5
9	1572	2.575	93.40	34.9	32.5
10	1546	2.574	93.36	34.6	32.2
11	1637	2.577	93.37	34.6	32.1
12	1583	2.575	93.30	34.3	31.9
13	1596	2.575	93.38	34.2	31.7
14	1648	2.577	93.42	34.5	31.9
15	1564	2.573	93.38	34.4	32.0
16	1579	2.574	93.38	34.3	31.9

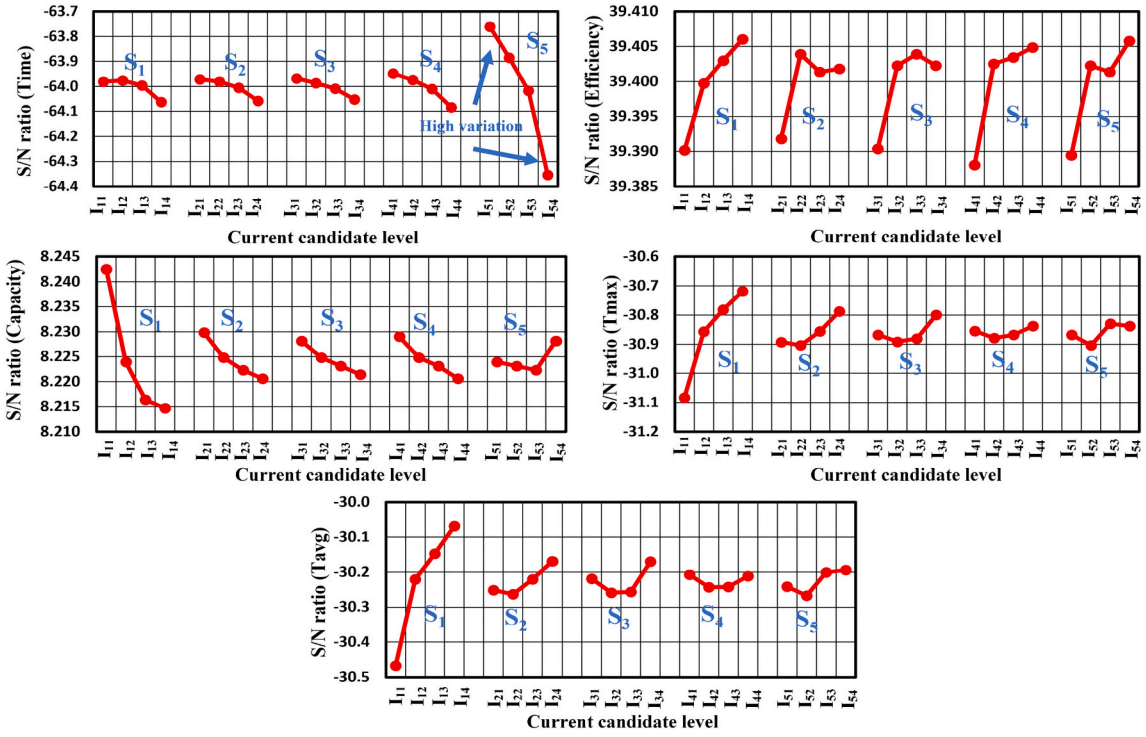

Fig. 9. Average S/N values of each current candidate for each performance parameters in second OA experiments.

Table 10
Comparison among selective performance based optimized charging profiles.

Charge method	Charge current (C-rate)		Charge time (%)	Charged capacity (%)	Energy efficiency (%)	Avg. temp. rise (%)	Max. temp. rise (%)
Time	S1	3.65	100.0 %	99.8 %	99.9 %	104.8 %	103.4 %
	S2	2.7					
	S3	2.1					
	S4	1.7					
	S5	0.9					
Charged capacity	S1	3.7	108.4 %	100.0 %	99.8 %	113.8 %	110.2 %
	S2	2.7					
	S3	2.1					
	S4	1.7					
	S5	0.7					
Energy efficiency and avg. temp	S1	3.5	113.5 %	99.9 %	100.0 %	100.0 %	103.4 %
	S2	2.65					
	S3	1.9					
	S4	1.5					
	S5	0.7					
Max. temp	S1	3.5	112.8 %	99.9 %	99.9 %	104.8 %	100.0 %
	S2	2.5					
	S3	1.9					
	S4	1.7					
	S5	0.7					
MOO profile	S1	3.5	105.4 %	100.0 %	99.9 %	103.0 %	103.4 %
	S2	2.5					
	S3	1.9					
	S4	1.7					
	S5	0.9					

indicate that the MOO charging strategy reduces charging time by around 10 % at the expense of a 1.4 °C higher average temperature rise. Interestingly, the maximum rise in surface temperature remains approximately the same in both scenarios. The charging energy efficiency is 0.3 % higher in CCCV at 25 °C, but at 35 °C, it is 0.2 % lower than the MOO strategy. Additionally, the charged and discharged capacity in CCCV is greater, around 0.5 %, than the MOO strategy. Overall, there are variations in performance parameters between these two charging strategies.

The effect of a higher C-rate and a higher first-stage SOC interval resulted in better results when we compared the findings from our previous research [30]. The MSCC charging reduced the charging time when compared to CCCV but did not significantly enhance the other performance parameters [30]. Using a higher C-rate and higher first-stage SOC level has led to noticeable improvements in this case. Compared to CCCV charging, we have seen improvements in the maximum surface temperature, charging energy efficiency, and reduction in charging time.

In summary, the MOO charging profile reduced the charging time with comparable temperature rise, making it a promising option for

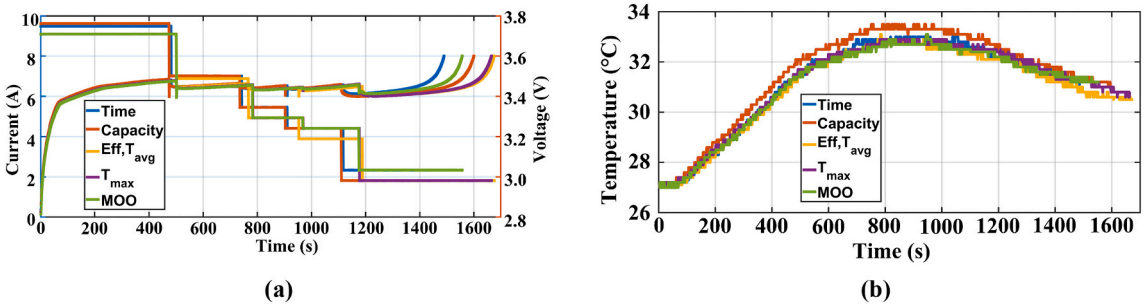

Fig. 10. Comparison of performance-based selective parameter charging profiles (charging time, capacity, Efficiency, T_{avg}, T_{max} and MOO charging) from second orthogonal set of experiments a) waveforms of battery voltage and implemented current levels for each performance parameter, b) demonstrating the optimization process's effect on battery temperature dynamics.

Table 11
Comparison between CCCV and 5SCC charging for each performance parameter.

Charge method	Charge current (C-rate)	Pre-set temp (°C)	Nominal charge capacity (%)	Nominal discharge capacity (%)	Charge time (s)	Energy efficiency (%)	Max. temp. rise (°C)	Avg. temp. rise (°C)
CCCV	2.262C to 3.6 V and 0.05C cut-off current	25	100	100	1758	93.4	7.8	4.1
5SCC (average 2.262 C)	S1 3.5 S2 2.5 S3 1.9 S4 1.7 S5 0.9	25	99.4	99.4	1578	93.1	7.7	5.5
CCCV	2.262C to 3.6 V and 0.05C cut-off current	35	100	100	1697	94.0	7.3	4
5SCC (average 2.262 C)	S1 3.5 S2 2.5 S3 1.9 S4 1.7 S5 0.9	35	99.5	99.5	1571	94.2	7.4	5.2

efficient EV charging, particularly in scenarios when the fast charging is prioritized.

5. Conclusion

Several charging methods have been proposed to enhance the performance of LIBs. The MSCC charging strategy has demonstrated potential for improving LIB's performance. However, performance parameters, such as charging time and surface temperature rise, may counteract each other when optimizing their performance. In other words, it is not straightforward to optimize all the parameters simultaneously. Therefore, the design of the MSCC charging strategy is, in fact, an optimization problem. Thus, the Taguchi method is used to identify the MOO charging profile. This method can address the challenges of developing complex models for LIB and significantly reduce the need for extensive and costly experimental testing.

This study systematically determines the optimal solutions for each performance parameter for the 5SCC charging strategy. To facilitate the analysis, a quality function is formulated to capture the relationship between the performance parameters and the charging current. The average effect of each charging current on the quality function at each stage is determined. After that, weighting factors are used to obtain the MOO charging profile. In addition, optimal solutions tailored to each performance parameter are determined. The customized charging patterns are experimentally validated. A comparison is made between the MOO charging profile and the equivalent CCCV method. The experimental results show that, at 25 °C, the MOO charging profile enables the LIB to charge 10.2 % faster than CCCV, although with a 1.4 °C higher average temperature rise and a 0.3 % decrease in energy efficiency. Furthermore, at 35 °C, the MOO charging profile accelerates LIB charging by 7.2 % compared to CCCV, with a 1.2 °C higher average temperature rise and a 0.2 % enhancement in charging energy efficiency. These findings highlight the effectiveness of the MSCC charging strategy, particularly in improving the outcomes at elevated temperatures. The MSCC reduced the charging time with a comparable surface maximum temperature rise to CCCV, making it an attractive option for efficient EV charging, particularly when fast charging is a priority. In addition, the effect of the optimized MSCC charging strategy on the LIB lifetime will be investigated in future publications.

CRediT authorship contribution statement

Muhammad Usman Tahir: Conceptualization, Data curation, Investigation, Methodology, Software, Visualization, Writing – original draft. **Ariya Sangwongwanich:** Investigation, Supervision, Visualization, Writing – review & editing. **Daniel-Ioan Stroe:** Investigation, Supervision, Visualization, Writing – review & editing. **Frede Blaabjerg:** Supervision, Writing – review & editing.

Declaration of competing interest

The authors declare that they have no known competing financial

interests or personal relationships that could have appeared to influence the work reported in this paper.

Data availability

Data will be made available on request.

References

[1] M.U. Tahir, M. Anees, H.A. Khan, I. Khan, N. Zaffar, T. Moaz, Modeling and evaluation of nickel manganese cobalt based Li-ion storage for stationary applications, J. Energy Storage 36 (2021) 102346.

[2] M.U. Tahir, T. Moaz, H.A. Khan, N.A. Zaffar, I. Khan, Accurate modeling of Li-ion cells applied to LiFePO 4 and NMC chemistries, in: 2020 IEEE Texas Power and Energy Conference (TPEC), 2020, pp. 1–6.

[3] P. Sun, R. Bisschop, H. Niu, X. Huang, A review of battery fires in electric vehicles, Fire. Technol 56 (2020) 1361–1410.

[4] J. Hong, Z. Wang, C. Qu, Y. Zhou, T. Shan, J. Zhang, Y. Hou, Investigation on overcharge-caused thermal runaway of lithium-ion batteries in real-world electric vehicles, Appl.Energy 321 (2022) 119229.

[5] T. Waldmann, B. Hogg, M. Wohlfahrt-Mehrens, Li plating as unwanted side reaction in commercial Li-ion cells–a review, J. Power Sources 384 (2018) 107–124.

[6] B.L. Rinkel, D.S. Hall, I. Temprano, C.P. Grey, Electrolyte oxidation pathways in lithium-ion batteries, J. Am. Chem. Soc. 142 (2020) 15058–15074.

[7] H. Oka, T. Nonaka, Y. Kondo, Y. Makimura, Quantification of side reactions in lithium-ion batteries during overcharging at elevated temperatures, J. Power Sources 580 (2023) 233387.

[8] A. Adam, J. Wandt, E. Knobbe, G. Bauer, A. Kwade, Fast-charging of automotive lithium-ion cells: in-situ lithium-plating detection and comparison of different cell designs, J. Electrochem. Soc. 167 (2020) 130503.

[9] X. Lin, K. Khosravinia, X. Hu, J. Li, W. Lu, Lithium plating mechanism, detection, and mitigation in lithium-ion batteries, Prog. Energy Combust. Sci. 87 (2021) 100953.

[10] D. Lee, B. Kim, C.B. Shin, Modeling fast charge protocols to prevent Lithium plating in a lithium-ion battery, J. Electrochem. Soc. 169 (2022) 090502.

[11] X. Huang, W. Liu, A.B. Acharya, J. Meng, R. Teodorescu, D. Stroe, Effect of pulsed current on charging performance of lithium-ion batteries, IEEE Trans. Ind. Electron. 69 (2021) 10144–10153.

[12] H. Beiranvand, N. Blasuttigh, T. Pereira, S. Hansen, H. Krueger, M. Liserre, A. M. Pavan, Charging strategy for lithium-ion batteries in V2G applications, in: 2022 IEEE Energy Conversion Congress and Exposition (ECCE), 2022, pp. 1–8.

[13] P. Keil, A. Jossen, Charging protocols for lithium-ion batteries and their impact on cycle life—an experimental study with different 18650 high-power cells, J. Energy Storage 6 (2016) 125–141.

[14] S. Hemavathi, A. Shinisha, A study on trends and developments in electric vehicle charging technologies, J. Energy Storage 52 (2022) 105013.

[15] Y. Li, J. Guo, K. Pedersen, L. Gurevich, D. Stroe, Investigation of multi-step fast charging protocol and aging mechanism for commercial NMC/graphite lithium-ion batteries, J. Energy Chem. 80 (2023) 237–246.

[16] L. Patnaik, A. Praneeth, S.S. Williamson, A closed-loop constant-temperature constant-voltage charging technique to reduce charge time of lithium-ion batteries, IEEE Trans. Ind. Electron. 66 (2018) 1059–1067.

[17] A.B. Khan, W. Choi, Optimal charge pattern for the high-performance multistage constant current charge method for the li-ion batteries, IEEE Trans. Energy Convers. 33 (2018) 1132–1140.

[18] F. An, R. Zhang, Z. Wei, P. Li, Multi-stage constant-current charging protocol for a high-energy-density pouch cell based on a 622NCM/graphite system, RSC Adv. 9 (2019) 21498–21506.

[19] M. Usman Tahir, A. Sangwongwanich, D. Stroe, F. Blaabjerg, Overview of multi-stage charging strategies for Li-ion batteries, J. Energy Chem. 84 (2023) 228–241.

[20] M.U. Tahir, A. Sangwongwanich, D. Stroe, F. Blaabjerg, The effect of multi-stage constant current charging on lithium-ion battery's performance, in: 2023 IEEE 17th International Conference on Compatibility, Power Electronics and Power Engineering (CPE-POWERENG), 2023, pp. 1–6.

[21] S. Wang, Y. Liu, A PSO-based fuzzy-controlled searching for the optimal charge pattern of Li-ion batteries, IEEE Trans. Ind. Electron. 62 (2014) 2983–2993.

[22] Y. Liu, J. Teng, Y. Lin, Search for an optimal rapid charging pattern for lithium-ion batteries using ant colony system algorithm, IEEE Trans. Ind. Electron. 52 (2005) 1328–1336.

[23] Y. Li, K. Li, Y. Xie, B. Liu, J. Liu, J. Zheng, W. Li, Optimization of charging strategy for lithium-ion battery packs based on complete battery pack model, J. Energy Storage 37 (2021) 102466.

[24] G. Chen, Y. Liu, S. Wang, Y. Luo, Z. Yang, Searching for the optimal current pattern based on grey wolf optimizer and equivalent circuit model of Li-ion batteries, J. Energy Storage 33 (2021) 101933.

[25] R. Mathieu, O. Briat, P. Gyan, J. Vinassa, Fast charging for electric vehicles applications: numerical optimization of a multi-stage charging protocol for lithium-ion battery and impact on cycle life, J. Energy Storage 40 (2021) 102756.

[26] X. Wu, Y. Xia, J. Du, X. Gao, S. Nikolay, Multi-stage constant current charging strategy based on multi-objective current optimization, in: IEEE Trans. Transp. Electrification, 2022.

[27] T.T. Vo, X. Chen, W. Shen, A. Kapoor, New charging strategy for lithium-ion batteries based on the integration of Taguchi method and state of charge estimation, J. Power Sources 273 (2015) 413–422.

[28] C. Lee, T. Chang, S. Hsu, J. Jiang, Taguchi-based PSO for searching an optimal four-stage charge pattern of Li-ion batteries, J. Energy Storage 21 (2019) 301–309.

[29] L. Jiang, Y. Li, Y. Huang, J. Yu, X. Qiao, Y. Wang, C. Huang, Y. Cao, Optimization of multi-stage constant current charging pattern based on Taguchi method for Li-ion battery, Appl. Energy 259 (2020) 114148.

[30] M.U. Tahir, A. Sangwongwanich, D.-I. Stroe, F. Blaabjerg, Optimized multi-stage constant current charging strategy for Li-ion batteries, in: 2023 25th European Conference on Power Electronics and Applications (EPE'23 ECCE Europe), 2023, pp. 1–9.

[31] D. Stroe, M. Swierczynski, A. Stroe, S. Knudsen Kær, Generalized characterization methodology for performance modelling of lithium-ion batteries, Batteries 2 (2016) 37.

[32] C. Lee, C. Hsu, S. Hsu, J. Jiang, Effect of weighting strategies on Taguchi-based optimization of the four-stage constant current charge pattern, IEEE Trans. Aerospace Electron. Syst. 57 (2021) 2704–2714.

[33] J.M. Amanor-Boadu, A. Guiseppi-Elie, E. Sánchez-Sinencio, Search for optimal pulse charging parameters for Li-ion polymer batteries using Taguchi orthogonal arrays, IEEE Trans. Ind. Electron. 65 (2018) 8982–8992.